UNCLASSIFIED

AD NUMBER

ADB013221

NEW LIMITATION CHANGE

TO

Approved for public release, distribution unlimited

FROM

Distribution authorized to U.S. Gov't. agencies only; Test and Evaluation; AUG 1976. Other requests shall be referred to Ballistic Research Labs., Aberdeen Proving Ground, MD.

AUTHORITY

BRL ltr, 13 Nov 1986

THIS PAGE IS UNCLASSIFIED

BRL

MEMORANDUM REPORT NO. 2655

QUASI-STATIC COMPRESSION STRESS-STRAIN
CURVES--IV, 2024-T3510 AND 6061-T6
ALUMINUM ALLOYS

Ralph F. Benck
Gordon L. Filbey, Jr.
E. Allen Murray, Jr.

August 1976

USA BALLISTIC RESEARCH LABORATORIES
ABERDEEN PROVING GROUND, MARYLAND

REPORT DOCUMENTATION PAGE		READ INSTRUCTIONS BEFORE COMPLETING FORM
1. REPORT NUMBER BRL Memorandum Report No.2655	2. GOVT ACCESSION NO.	3. RECIPIENT'S CATALOG NUMBER
4. TITLE *(and Subtitle)* Quasi-Static Compression Stress-Strain Curves--IV, 2024-T3510 and 6061-T6 Aluminum Alloys		5. TYPE OF REPORT & PERIOD COVERED Final
		6. PERFORMING ORG. REPORT NUMBER
7. AUTHOR(s) Ralph F. Benck Gordon L. Filbey, Jr. E. Allen Murray, Jr.		8. CONTRACT OR GRANT NUMBER(s)
9. PERFORMING ORGANIZATION NAME AND ADDRESS USA Ballistic Research Laboratories Aberdeen Proving Ground, MD 21005		10. PROGRAM ELEMENT, PROJECT, TASK AREA & WORK UNIT NUMBERS RDT&E Proj. No. 1T161102A33H
11. CONTROLLING OFFICE NAME AND ADDRESS US Army Materiel Development & Readiness Command 5001 Eisenhower Avenue Alexandria, VA 22333		12. REPORT DATE AUGUST 1976
		13. NUMBER OF PAGES 31
14. MONITORING AGENCY NAME & ADDRESS *(if different from Controlling Office)*		15. SECURITY CLASS. *(of this report)* Unclassified
		15a. DECLASSIFICATION/DOWNGRADING SCHEDULE

16. DISTRIBUTION STATEMENT *(of this Report)*

Distribution limited to US Government agencies only; Test and Evaluation; August 1976. Other requests for this document must be referred to Director, USA Ballistic Research Laboratories, ATTN: DRXBR-TS, Aberdeen Proving Ground, Maryland 21005.

17. DISTRIBUTION STATEMENT *(of the abstract entered in Block 20, if different from Report)*

18. SUPPLEMENTARY NOTES

19. KEY WORDS *(Continue on reverse side if necessary and identify by block number)*

armor
yield strength
Poisson's ratio
compressibility

Young's modulus
stress-strain curves
aluminum alloy

20. ABSTRACT *(Continue on reverse side if necessary and identify by block number)*

This report presents results of quasi-static compression tests of 2024-T3510 and 6061-T6 aluminum alloy rods performed at $22^{\circ}C$. The yield strengths, Poisson's ratios and Young's moduli are reported. An analysis of the variation of Poisson's ratio with strain, based on classical plasticity assumption, is presented and compared with the tests. In light of these test results, the necessity for a reinterpretation of the compressibility of metals accompanying plastic flow is demonstrated.

TABLE OF CONTENTS

Page

I. INTRODUCTION

The quasi-static compression tests reported herein were conducted in connection with the Core Materials Program of the Solid Mechanics Branch of the Terminal Ballistics Laboratory.

The purpose of the Core Materials Program is to characterize the mechanical behavior of armor and armor penetrators. This characterization should prove useful to designers of armored vehicles and projectiles, and will provide valuable input data for computer codes modeling penetration processes.

This report presents the results of quasi-static compression tests on two aluminum alloys; 2024-T3510, and 6061-T6. These results include the yield strength, average stress-strain curve, Poisson's ratio, and Young's moduli for each aluminum alloy.

These two materials are the fourth and fifth in a series[1,2,3] which includes seven steel and seven aluminum alloys*. The results of other tests will follow when completed.

II. TEST PROCEDURES

The testing apparatus, procedures and data reduction regimen have been reported previously[1]. The test specimens of each material were machined from one-inch diameter rods of commercial purity. Six test specimens of each material were prepared as right circular cylinders, 9.5mm in diameter and 28.6mm long. Samples of both materials were chemically analyzed at the Frankford Arsenal. The temperature for the tests was 22°C.

---

[1]E. A. Murray, Jr. and J. H. Suckling, BRL MR 2399, "Quasi-Static Compression Stress-Strain Curves--I, 1066 Steel", Ballistics Research Laboratories, APG, MD., January 1974. AD 922 704 L.

[2]E. A Murray, Jr., BRL MR 2589, "Quasi-static Compression Stress-Strain Curves--II, 7039 Aluminum," Ballistics Research Laboratories, APG, MD. February 1976. AD #B0009646L.

[3]Ralph F. Benck and E. A Murray, Jr., BRL MR 2480, "Quasi-Static Compression Stress-Strain Curves--III, 5083-H131 Aluminum", Ballistics Research Laboratories, APG, MD. May 1975. AD B00 4159 L.

*Steel Alloys: 1020, 1066, 4145, 4160, 4340, Bearcat, and RHA. Aluminum Alloys: 1100F, 2024-T3510, 5083-H131, 6061-T6, 7039, 7075, and 7475.

III. RESULTS

The average engineering stress-strain curves for six specimens each of 2024-T3510 and 6061-T6 aluminum alloy are shown in Figures 1 and 2, respectively. The vertical error bands in the figures are the variations of stress of plus and minus one standard deviation. The tests were terminated upon failure of one of the strain gages. Table I shows the maximum strain attained prior to gage failure. The curves presented in Figures 1 and 2 are the averages from at least two tests.

Figures 3 and 4 present longitudinal and circumferential stress-strain relationships for a representative specimen each of the 2024-T3510 and 6061-T6 aluminum alloy material.

The curves labeled "longitudinal" in Figures 3 and 4 indicate both the individual response of each of two diametrically opposing gages as well as their average. The average value is the longitudinal strain in the specimen at any load (~stress), and divergence from this average is indicative of the amount of bending present. The near coalescence of the curves for individual gages with their average in each test demonstrates the high degree of axiality maintained throughout these compression tests.

Poisson's ratios as a function of strain for these two alloys are similar; examples of Poisson's ratio up to one and up to five percent strain are shown in Figures 5 and 6, respectively. Poisson's ratio for both alloys is 0.32 in the elastic region and approaches 0.5 as the material becomes more and more plastic.

The average yield strength, Young's modulus and Poisson's ratio for the 2024-T3510 and 6061-T6 alloys are presented in Table II. The number within the parentheses is the standard deviation based on six tests of each alloy. The yield strength is defined as that stress at which the specimens deviated 0.2 percent from proportionality of stress to strain[4].

The results of chemical analyses of samples of both alloys are shown in Table III.

---

[4]*Taylor Lyman, Ed., Metals Handbook, 1948 Edition, The American Society for Metals, Cleveland, Ohio, p. 16.*

TABLE I

MAXIMUM STRAIN PRIOR TO GAGE FAILURE

SPECIMEN	2024-T3510 %	6061-T6 %
1	7.26	8.54
2	7.37	4.68
3	9.37	6.04
4	9.76	4.75
5	8.31	4.87
6	3.39	8.12

TABLE II

MEASURED MATERIAL PROPERTIES
OF 2024-T3510 AND 6061-T6 ALUMINUM ALLOYS AT 22°C

PROPERTY	2024-T3510	6061-T6
Average Yield Strength, MPa ⟨S.D.⟩ *	444 ⟨5.1⟩	267 ⟨2.3⟩
Young's modulus, GPa ⟨S.D.⟩ *	76.1 ⟨0.9⟩	72.2 ⟨0.7⟩
Poisson's ratio	0.321	0.320
Hardness, BHN	148	95

*S.D. = Standard Deviation

TABLE III

CHEMICAL ANALYSIS OF 2024-T3510 AND
6061-T6 ALUMINUM ALLOYS*

ELEMENT	WEIGHT PERCENT	
	2024-T3510	6061-T6
Copper	4.20	0.2/0.4
Silicon	0.1/0.2	0.4/0.8
Iron	0.2/0.4	0.15/0.35
Manganese	0.4/0.8	0.06
Zinc	0.05/0.15	<0.1
Magnesium	1.50	1.11
Titanium	<0.05	<0.05
Chromium	<0.03	0.10/0.25
Nickel	<0.02	<0.01
Tin	None detected	None detected
Lead	<0.05	0.05, <0.05
Aluminum	Remainder	Remainder

*Analysis by Frankford Arsenal, Materials Laboratory, Technical
Support Directorate. Spectroscopic Analysis.

An analytical relationship between Poisson's ratio and strain over
the range depicted in Figure 6 has not been documented, or at least no
references to such a relationship have been found. While the initial
(elastic) and final (0.5) values have been amply discussed in texts and
the literature, the form for Poisson's ratio in the region between onset
of yielding and final values has never been formalized. Yet in principle,
if the claims of classical plasticity theory concerning incompressible
plastic deformations are correct, the transition in Poisson's ratio from
elastic value to asymptotic large plastic value should be orderly and
predictable from the longitudinal stress-strain curve. In an effort to
add to the understanding of information such as that presented in Figure 6,
an analytical relationship between Poisson's ratio and longitudinal strain,
based on incompressible plasticity, is developed in the Appendix. It is
expressed as:

$$\nu_{apparent} = \frac{\hat{\sigma}}{\varepsilon_{xx}(\hat{\sigma})}\left(\frac{\nu_e - 1/2}{E}\right) + \frac{1}{2} \qquad (1)$$

where

$\nu_{apparent}$ = Poisson's ratio in plastic region

$\hat{\sigma}$ = longitudinal stress

$\varepsilon_{xx}(\hat{\sigma})$ = longitudinal strain at $\hat{\sigma}$ stress

$$\nu_e = \text{Poisson's ratio determined from static tests via extrapolation to zero strain.}$$

$$E = \text{Young's modulus determined from static test via "best fit" in linear elastic region.}$$

In developing (1) it has been assumed that the "plastic" component of strain is incompressible, viz.

$$\frac{\varepsilon_{\theta\theta}(\hat{\sigma}) - \dfrac{\hat{\sigma}\nu_e}{E}}{\varepsilon_{xx}(\hat{\sigma}) - \dfrac{\hat{\sigma}}{E}} = 1/2 \qquad (2)$$

All terms in Equation 2 are as defined for Equation 1, and $\varepsilon_{\theta\theta}(\hat{\sigma})$ is the circumferential strain at longitudinal stress $\hat{\sigma}$.

$\nu_{apparent}$ and $\nu_{predicted}$ are plotted in Figure 7 versus ε_{xx} for one sample of 2024-T3510 alloy. For these calculations the measured values of E and ν (76.588 GPa and 0.323 respectively) for this particular test were used and not the average values shown in Table II. $\nu_{apparent}$ is Poisson's ratio calculated from the ratio of the experimentally measured longitudinal and circumferential strains.

Figure 7 shows that expression (1) is an accurate predictor of Poisson's ratio for the rapidly ascending portion of the curve. For the remainder of Figure 7 the curves separate with the maximum separation being about five percent. The five other samples of 2024-T3510 and those of 6061-T6 that are reported herein yielded curves similar to those shown in Figure 7 with the difference between $\nu_{apparent}$ and $\nu_{predicted}$ at strains greater then two percent being in the order of plus or minus six percent.

In lieu of assuming an incompressible plastic component of the deformation and linear work hardening, one may in fact, take the other point of view and use the test data of this report to compute the material compressibility as a function of stress or strain. In this way, a separate check is made on the final assumptions of the analytical development in the Appendix.

Continue to assume homogeneous deformation and stress states as put forth in the Appendix. Consistent with notation introduced there, the initial and final volumes of a cylinder are $V_o = \pi\, r_o^2\, l_o$ and $V_1 = \pi(r^{\prime})^2 (1+\varepsilon_{xx})\, l_o = \pi\, r_o^2\, (1+\varepsilon_{\theta\theta})^2\, (1+\varepsilon_{xx})\, l_o$. Hence one easily has for the compressibility

$$\frac{\Delta V}{V_o} = \frac{V_1 - V_o}{V_o} = \left[(1 + \varepsilon_{\theta\theta})^2 \ (1 + \varepsilon_{xx}) - 1 \right] \qquad (3)$$

The Poisson's ratio vs. strain data of Figures 5, 6, and 7 coupled with Appendix Equation A-4 may be used to recover the observed variable $\varepsilon_{\theta\theta}$ as a function of ε_{xx}. Equation (3) expresses the compressibility $\frac{\Delta V}{V_o}$ implicity as a function of stress; the functional form may be made an explicit function of σ by means of the experimentally determined stress-strain relation $\varepsilon = \varepsilon(\hat{\sigma})$. Thus one may plot $\frac{\Delta V}{V_o}$ as a function of σ, and this should be the most instructive manner in which to view this interdependence. For, a consequence of the development in the Appendix is that only the current value of the elastic component of strain (in the elastic-plastic decomposition) contributes to volume change. Since this is taken to be linearly related to longitudinal stress, equal stress increments should cause equal volume change increments.

Figure 8 shows a plot of the compressibility $\frac{\Delta V}{V_o}$ as a function of stress, calculated by means of Equation 3 and the stress-strain curve for the same test that was used to derive Figure 7. The compressibility is nearly linear from the origin to a point whose stress value is 465 MPa. Note the radical departure in the compressibility curve from the linear one at 465 MPa, as well as the first detectable departure at 425 MPa. Interestingly enough, the behavior beyond 465 MPa is nearly linear also, but at a much reduced modulus of compressibility. It is also noteworthy that the strain corresponding to 465 MPa is well beyond the "knee" of the stress-strain curve of Figure 1, and corresponds to a strain of 1.10 percent. The proportional limit is closer to 425 MPa, the first detectable departure point in Figure 8, with corresponding strain 0.59 percent. These two observations are consistent with the extremely close agreement between apparent (measured) and predicted values of Poisson's ratio up to 1.10 percent strain in Figure 7. Although the differences beyond this strain were within ±6 percent, they are now known to be related to the radical change in compressibility at 1.10 percent longitudinal strain.

At this point, it is conjecture as to the causes of (1) the radical change in material compressibility noted here and (2) its delayed occurrence well beyond the proportional limit. The results, however, are not inconsistent with empirical multi-stress component plasticity theories of Bell[5] as to regions of onset of total plasticity and the transition strains. Further investigations will be reported at a later date.

---

[5]*James F. Bell, BRL CR 250, "A New, General Theory of Plasticity for Structural Metal Alloys", Ballistics Research Laboratories, APG, MD, July 1975. AD #A014192L.*

10

IV. CONCLUSIONS

Quasi-static compression tests were made on 2024-T3510 and 6061-T6 aluminum alloys. The data acquired from these tests have been reduced and are in a form readily applicable for users.

It is evident from the reproducibility of the data, that the results presented are an accurate, partial description of the elastic and plastic properties of 2024-T3510 and 6061-T6 aluminum alloys.

An analytical expression has been developed that accurately predicts the behavior of Poisson's ratio as a function of strain in the strain region beyond the proportional limit.

Well beyond the proportional elastic limit, a radical change occurs in the compressibility of each of these two alloys, and is the point of demarcation where the above analytical prescription begins to develop errors of ±6 percent. The compressibility may relate to newer empirical constitutive equations developed by Bell (see Reference 5), but such a connection is speculative at this point.
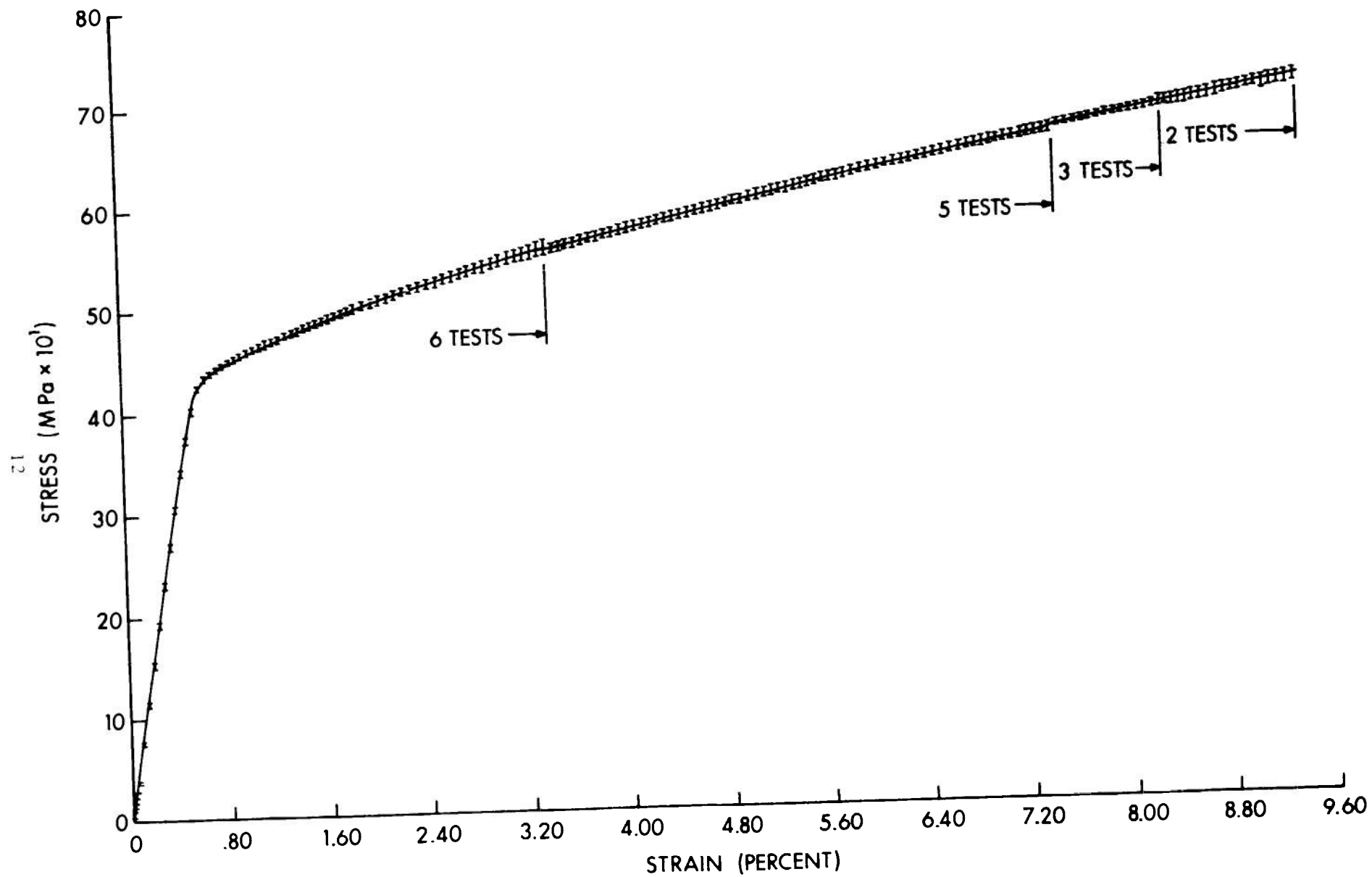
Figure 1. Average Stress - Strain Curve for Compression Test of 2024 T 3510 Aluminum.
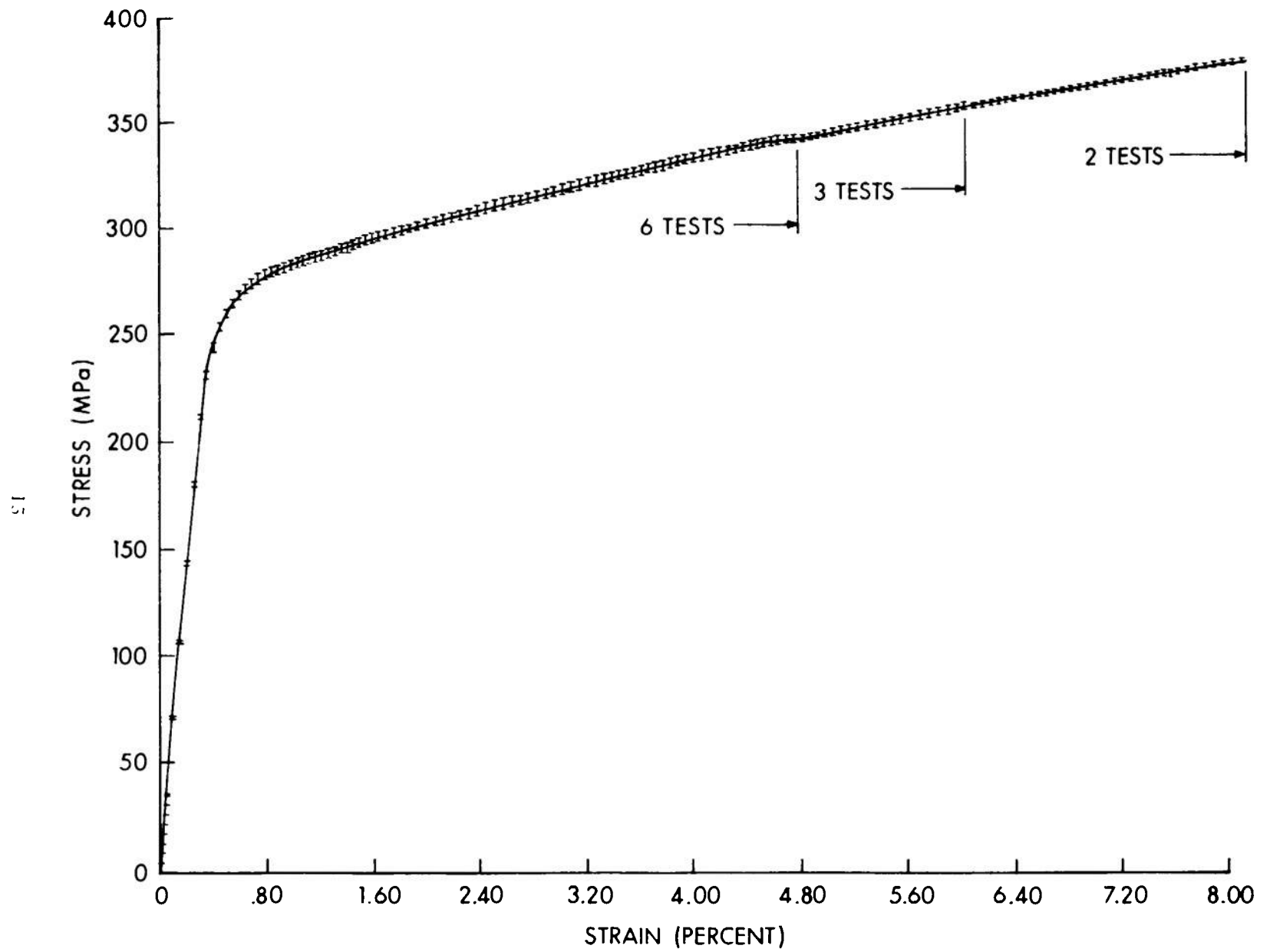
Figure 2. Average Stress-Strain Curves for Compression Test of 6061 T6 Aluminum.
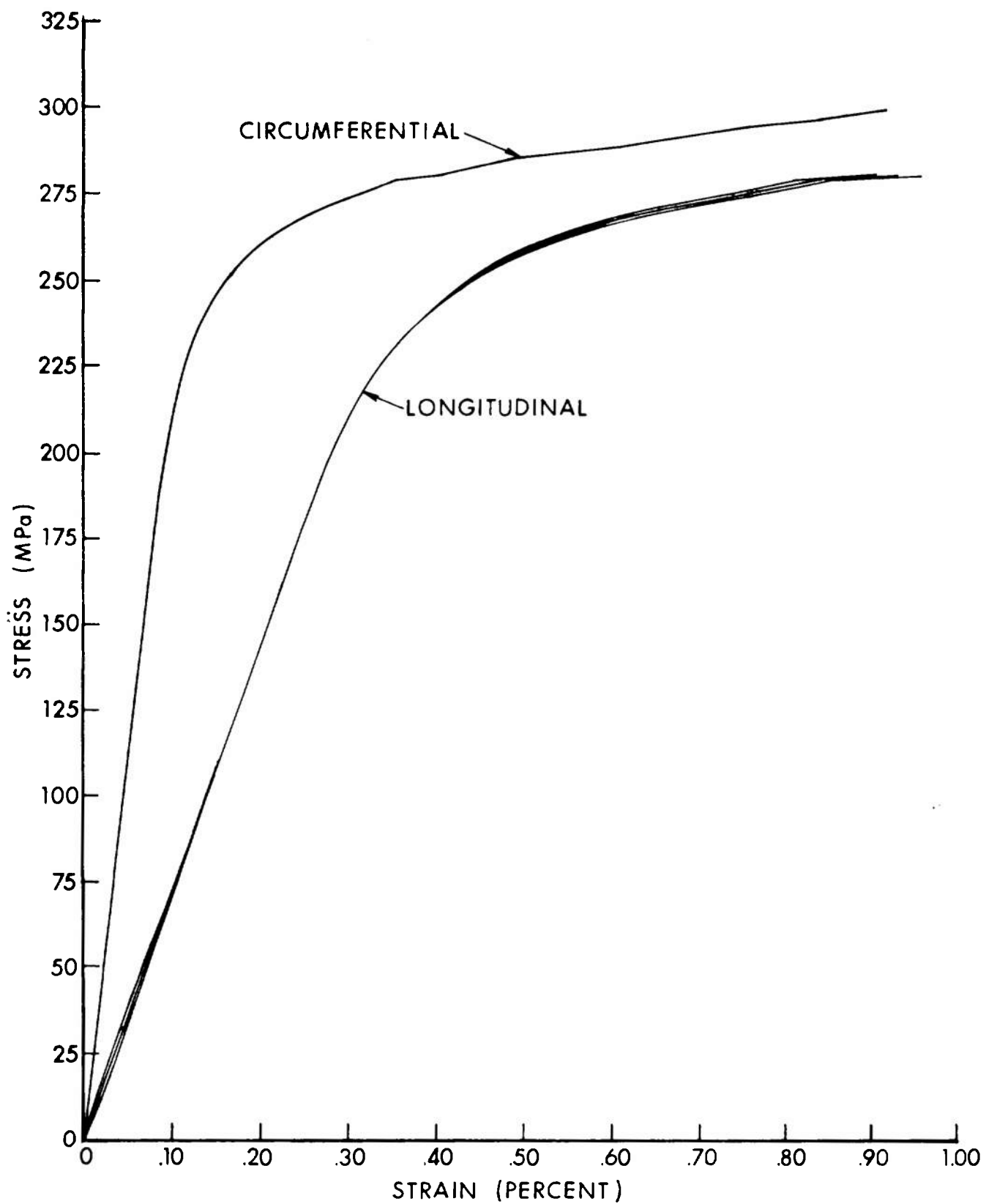
Figure 4. Stress-Strain Curves for One Specimen of 6061 T6 Aluminum.

14
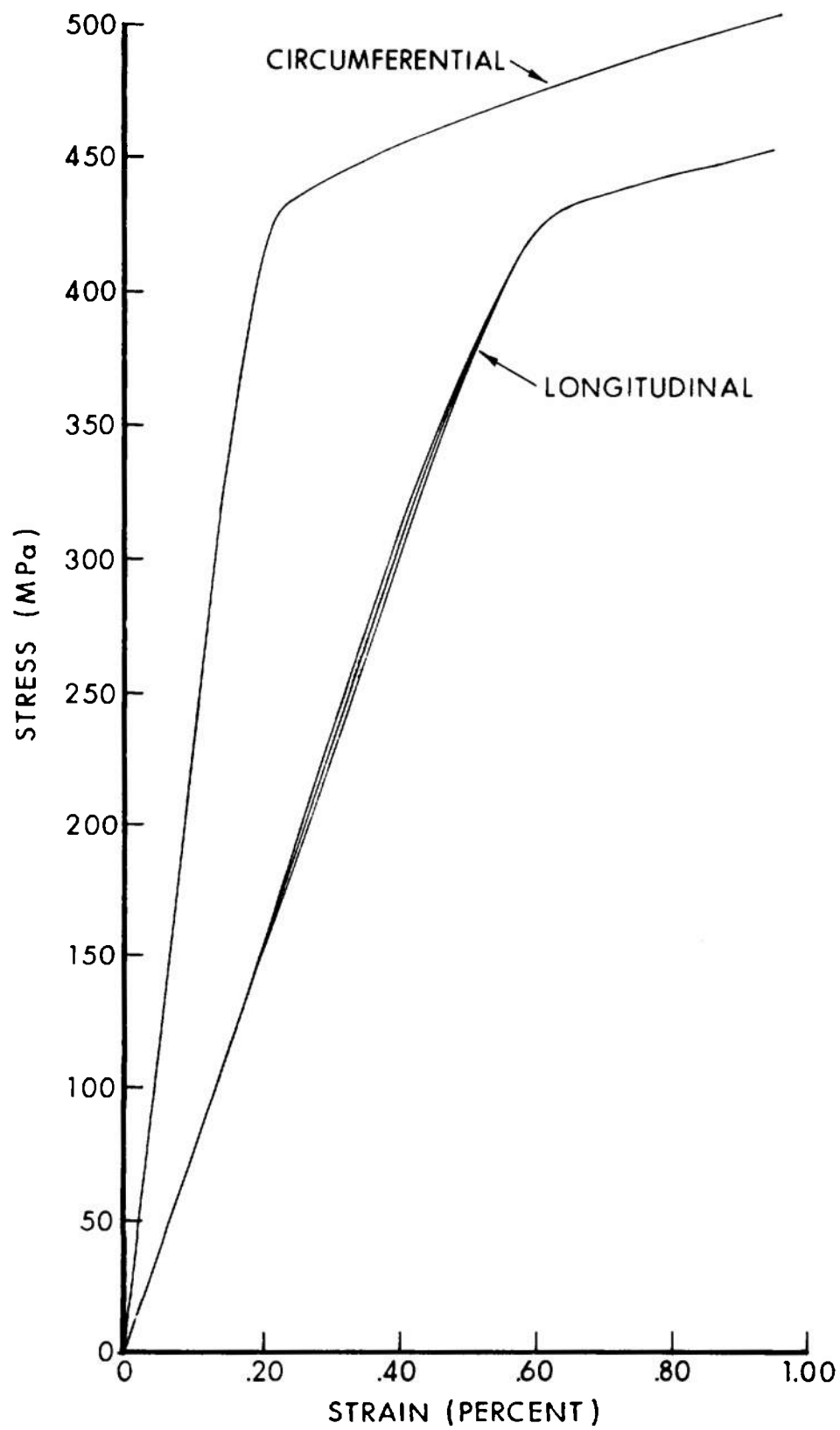
Figure 3. Stress-Strain Curves for One Specimen
of 2024 T3510 Aluminum
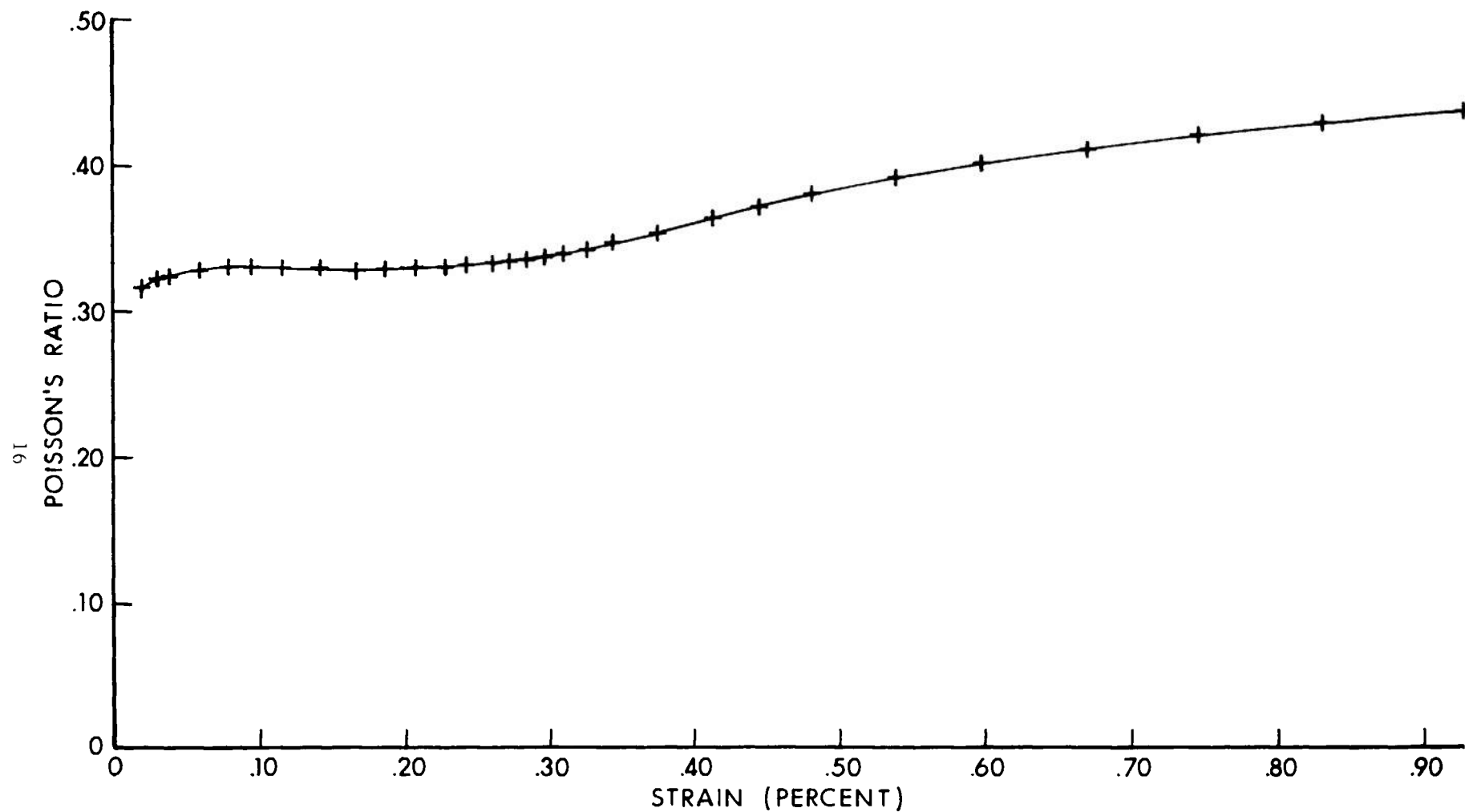
Figure 5.   Poisson's Ratio as a Function of Strain up to One Percent Maximum Strain for 6061 T6 Aluminum.
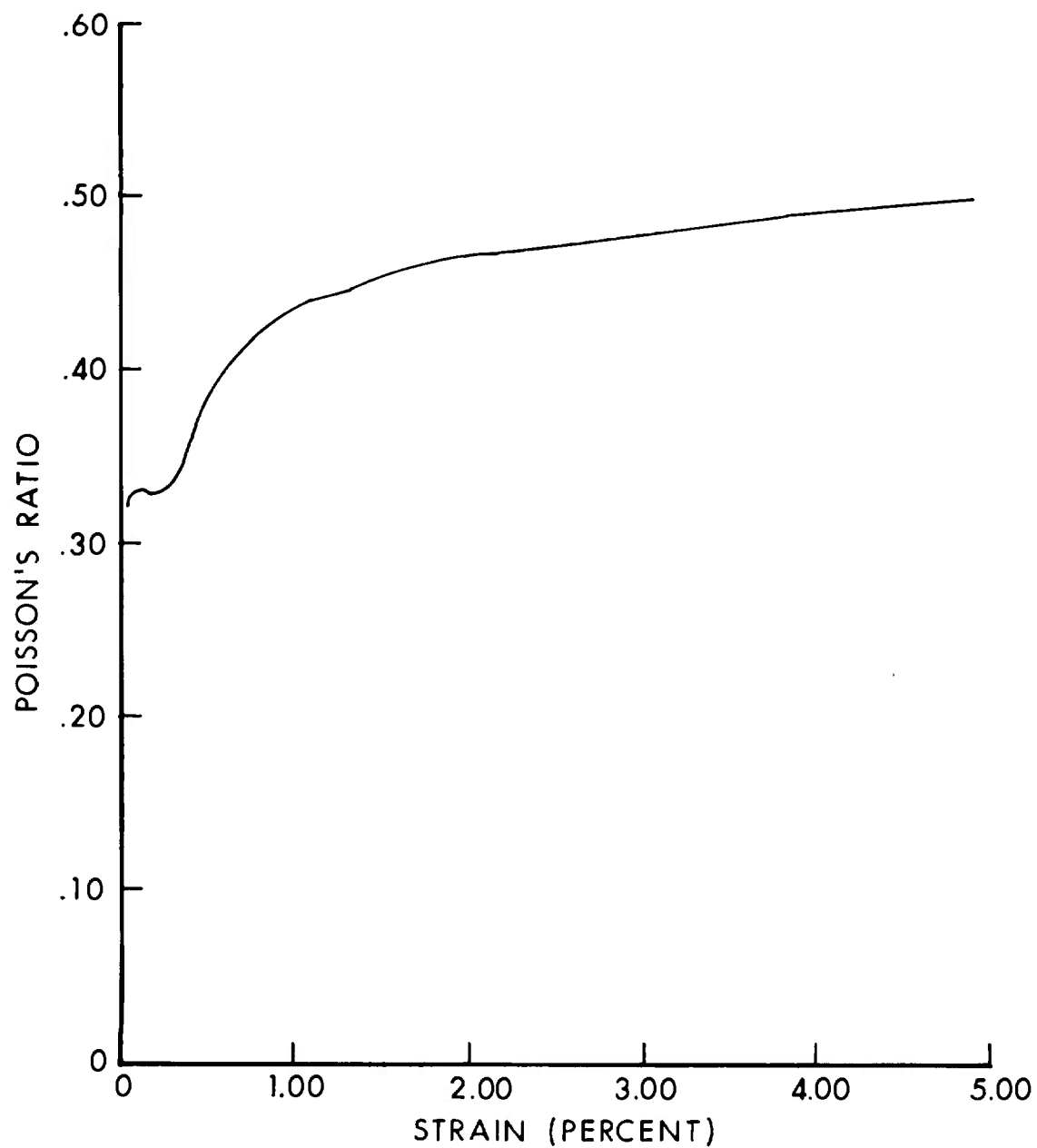
Figure 6. Poisson's Ratio as a Function of Strain up to Five Percent Maximum Strain for 6061 T6 Specimen.
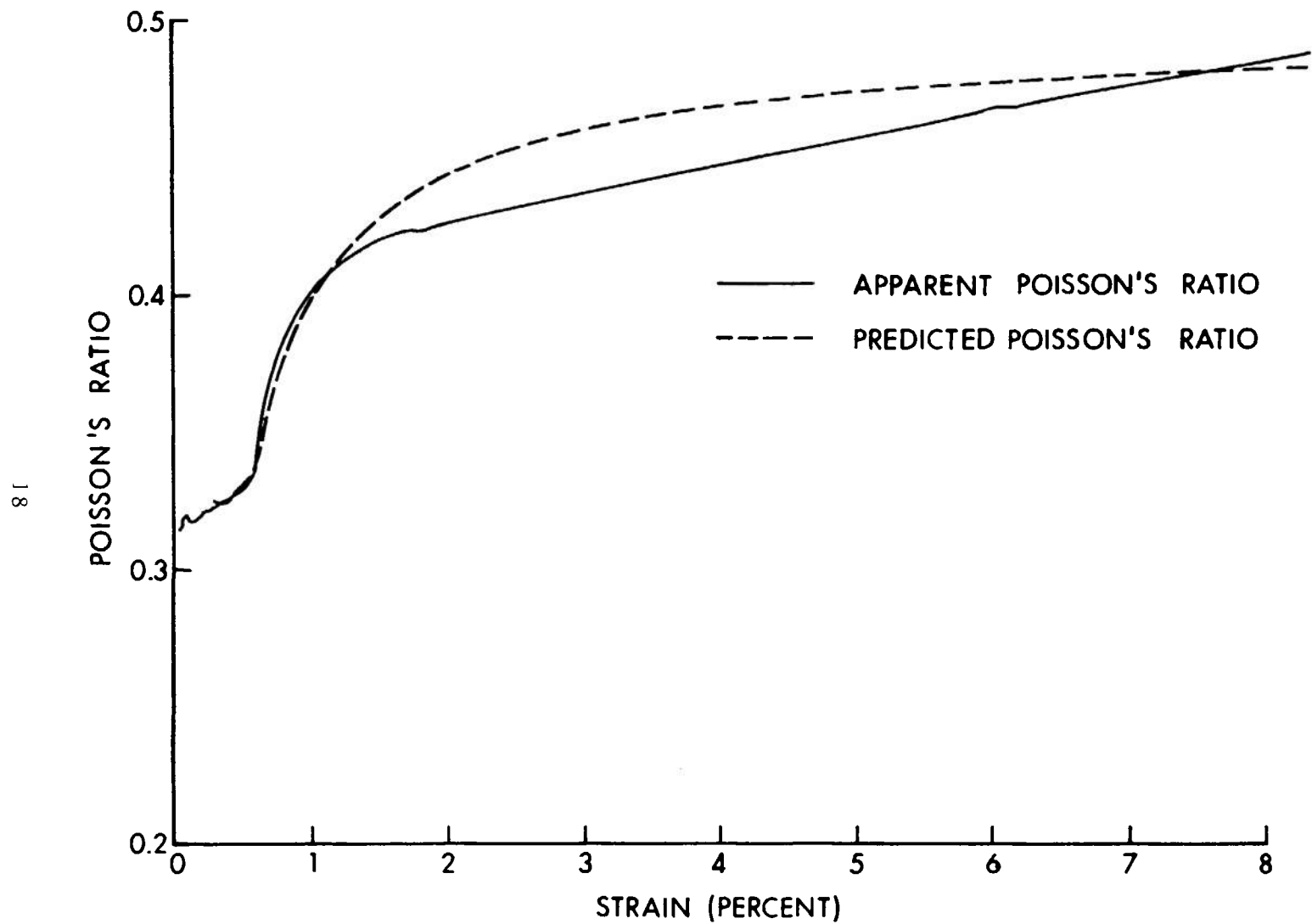
Figure 7. Predicted and Apparent Poisson's Ratio as a Function of Strain for 2024 T3510 Specimen.
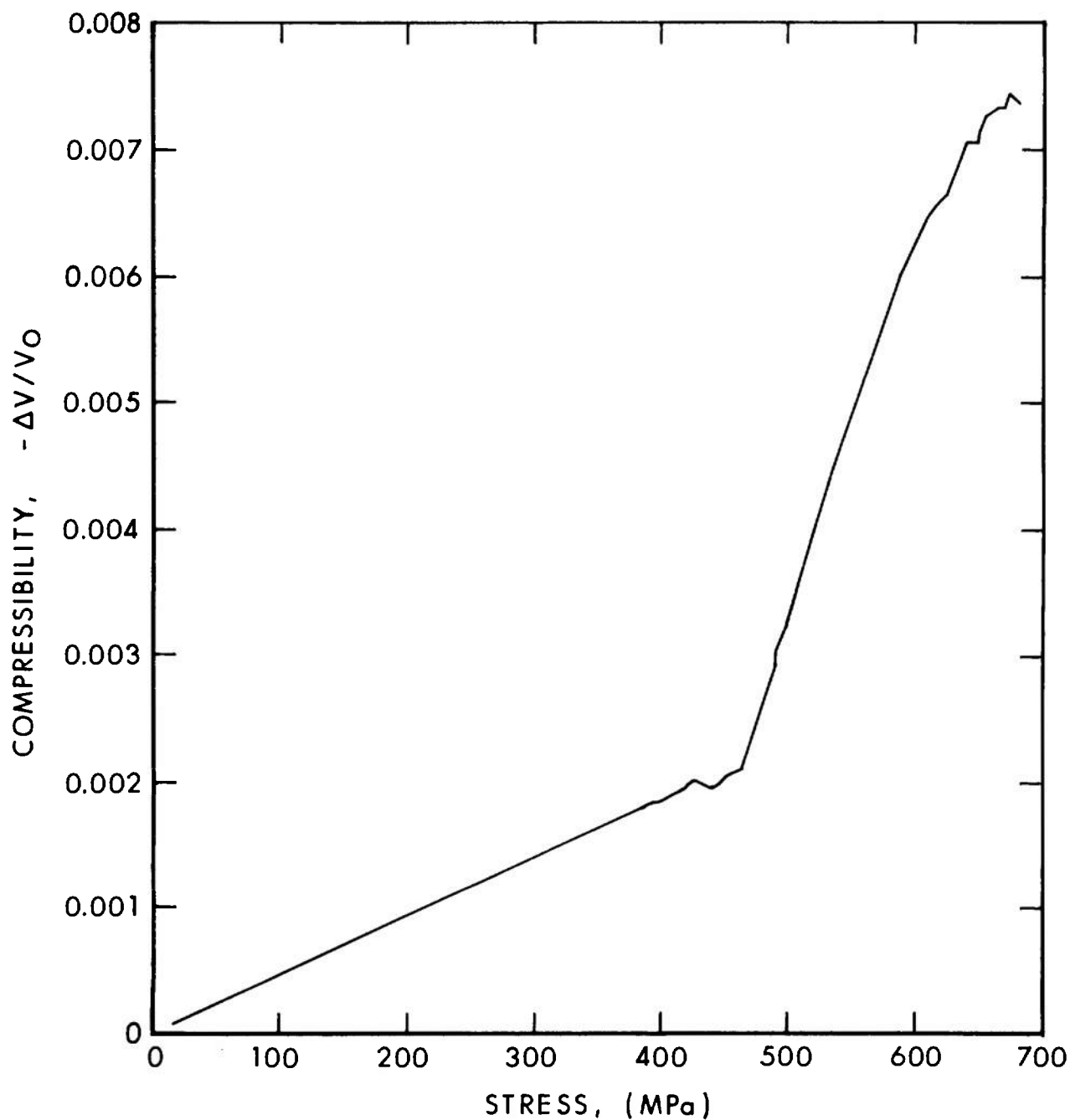
Figure 8.   Compressibility as a Function of Stress
for 2024 - T3510 Specimen.

APPENDIX

POISSON'S RATIO AS A FUNCTION OF STRAIN

APPENDIX

An expression for the apparent Poisson's ratio in the strain region beyond the linear elastic limit and preceding large plastic deformations (> 10%) will be developed. Consider the homogeneous deformation of a right circular cylinder of material as should be experienced in laboratory uni-axial tension or compression testing. Assume that plane sections normal to the x axis in the accompanying sketch remain plane, and that the strain fields are homogeneous in x and r, and independent of θ. The apparent Poisson's ratio, ν_{app}, in such an experiment is defined as the ratio of radial contraction to longitudinal extension, normalized to strain measures. That is, if the cylinder sketched is of initial length l_o and radius r_o, and the longitudinal extension is u_x and the accompanying radial motion is u_r (positive if outward), then
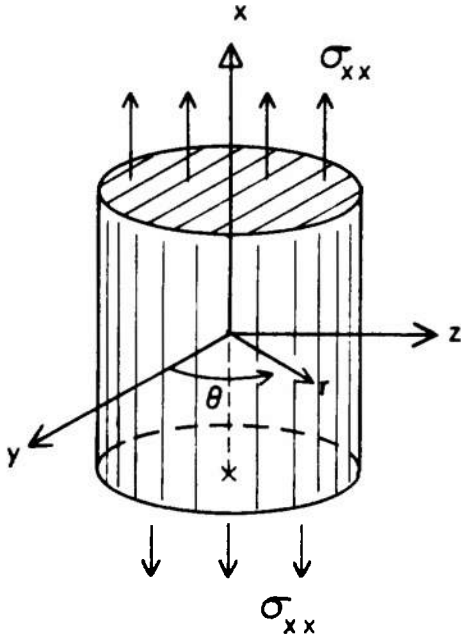
$$\nu_{app} = - \frac{u_r/r_o}{u_x/l_o} \qquad (A-1)$$

The longitudinal "engineering" strain ε_{xx} is recognized as the denominator u_x/l_o, and would be the quantity measured by a longitudinal strain gage. The quantity in the numerator, u_r/r_o, is the "hoop" engineering strain $\varepsilon_{\theta\theta}$. Let r_o be the initial radius of the cylindrical surface, and $r' = r_o + u_r$ the radius after some homogeneous deformation. Then the hoop engineering strain would be circumferential strain

$$\varepsilon_{\theta\theta} = \frac{2\pi r' - 2\pi r_o}{2\pi r_o} = \frac{u_r}{r_o} \qquad (A-2)$$

This is the quantity which would be measured by a strain gage oriented in the "hoop" direction. Thus, the apparent Poisson's ratio is determined by:

$$\nu_{app} = - \frac{\varepsilon_{\theta\theta}}{\varepsilon_{xx}} \qquad (A-3)$$

A typical stress-strain curve for materials of interest would have the form represented in the second sketch. Plotted also on this sketch is the negative value of the hoop strain $\varepsilon_{\theta\theta}$. Since

the algebraic sign of $\varepsilon_{\theta\theta}$ will always be opposite that of ε_{xx}, suppress the (-) sign in the ensuing argument and treat the plotted variables as if they are both of the same sign and positive. Thus Equation A-3 becomes for the purposes of this development

$$\nu_{app} = + \frac{\varepsilon_{\theta\theta}}{\varepsilon_{xx}} , \tag{A-4}$$

as plotted. A good first approximation to materials behavior is that of "plastic work hardening". This means among other things, that after loading the material beyond the linear elastic limit M, along MP to a stress $\hat{\sigma}$, the stress-strain curve will return along PR parallel to the loading modulus line OM upon unloading. The accompanying negative hoop strain will follow along some linear path ON, another presently unprescribed path NQ, and subsequently return along the linear path QS. Plastic work hardening also means that upon reloading, from R, the material will follow the linear modulus line, RP, to the previous unloading point P, and then proceed along the original curve, MPT, as if no unloading had occurred. It is the purpose of this Appendix to show that path NQ of the negative hoop strain beyond the proportional limit is indeed prescribed in a manner consistent with the assumptions of plastic work hardening and incompressible plasticity.

Define as a materials constant the ratio determined by experiment

$$\nu_e = \text{Materials Constant} = \frac{\varepsilon_{\theta\theta}^{(e)}}{\varepsilon_{xx}^{(e)}} \tag{A-5}$$

24

where $\varepsilon_{xx}^{(e)}$ and $\varepsilon_{\theta\theta}^{(e)}$ are the strains respectively at the points M and N, the proportional limit. This is, of course, the elastic value of Poisson's ratio. In the linear elastic region the connection between stress and longitudinal strain is

$$\sigma_{xx} = E\varepsilon_{xx} \tag{A-6}$$

where E is the usual Young's modulus. From the sketch and Equation A-5, a connection can also be written between stress and hoop strain in the linear elastic region as

$$\sigma_{xx} = E^* \, \varepsilon_{\theta\theta} = E^* \, \nu_e \, \varepsilon_{xx} \; , \tag{A-7}$$

where E^* is an apparent modulus. Comparing Equations A-6 and A-7 yields

$$E^* = \frac{E}{\nu_e} \tag{A-8}$$

Make strain decompositions into components, so that the total strain is the sum of an elastic and plastic component, expressed as

$\varepsilon_{xx} = \varepsilon_{xx}^{(e)} + \left(\varepsilon_{xx} - \varepsilon_{xx}^{(e)} \right)$. Equation A-4 may be written

$$\nu_{app} = \frac{\varepsilon_{\theta\theta}^{(e)} + \left(\varepsilon_{\theta\theta} - \varepsilon_{\theta\theta}^{(e)} \right)}{\varepsilon_{xx}^{(e)} + \left(\varepsilon_{xx} - \varepsilon_{xx}^{(e)} \right)} \tag{A-9}$$

But now assume plastic work hardening. This means that the elastic component is the elastic strain which would be recovered if unloading should occur from a stress $\hat{\sigma}$, even though it is not actually done. Hence, with Equation A-6 and A-7, Equation A-9 becomes

$$\nu_{app} = \frac{\dfrac{\hat{\sigma}}{E^*} + \left(\varepsilon_{\theta\theta}(\hat{\sigma}) - \dfrac{\hat{\sigma}}{E^*} \right)}{\dfrac{\hat{\sigma}}{E} + \left(\varepsilon_{xx}(\hat{\sigma}) - \dfrac{\hat{\sigma}}{E} \right)} \tag{A-10}$$

Equations (A-8) and (A-10) may be combined to yield

$$\nu_{app} = \frac{\dfrac{\hat{\sigma}\nu_e}{E} + \left(\varepsilon_{\theta\theta}(\hat{\sigma}) - \dfrac{\hat{\sigma}\nu_e}{E} \right)}{\hat{\sigma}/E + \left(\varepsilon_{xx}(\hat{\sigma}) - \hat{\sigma}/E \right)} \tag{A-11}$$

The expression is often heard, "Poisson's ratio for plastic deformation is equal to one-half". Assuming an incompressible homogeneous deformation of the cylinder sketched previously, and if the volume before deformation is $V_o = \pi r_o^2 \, l_o$ and following deformation is $V_1 = \pi (r´)^2 (1+\varepsilon_{xx}) l_o$, one finds that setting $V_o = V_1$ yields

$$r_o^2 = (r´)^2 (1+\varepsilon_{xx})$$

or that

$$\frac{r'}{r_o} = 1 + \frac{u_r}{r_o} = (1+\varepsilon_{xx})^{-\frac{1}{2}} \qquad \text{(A-12)}$$

$$= 1 - \frac{1}{2}\varepsilon_{xx} + \frac{3}{8}\varepsilon_{xx}^2 - \cdots$$

Thus, with Equation A-2, Equation A-12 becomes, for an incompressible deformation

$$\varepsilon_{\theta\theta} = -\frac{1}{2}\varepsilon_{xx}\left(1 - \frac{3}{4}\varepsilon_{xx} + \cdots\right) \qquad \text{(A-13)}$$

Comparing Equations A-13 and A-3, one sees that the apparent Poisson's ratio for a totally incompressible deformation is approximately 1/2, to a first order error correction of $O(3/4\ \varepsilon_{xx})$. This means that for a 4 percent longitudinal strain, Poisson's ratio differs from 1/2 by 3 percent. Since longitudinal strains of this order are discussed in this report, this level of error shall be accepted. However, Poisson's ratio is not 1/2 in the elastic region*, so that the assumption of total incompressibility from the initial state is inconsistent with reality.

Assume now, in the expression developed into Equation A-11, that the plastic component of the deformation is incompressible. Thus, within an error band of approximately 3 percent, by Equation A-13 one has

$$\left(\varepsilon_{\theta\theta}(\hat{\sigma}) - \frac{\hat{\sigma}\nu_e}{E}\right) = \frac{1}{2}\left(\varepsilon_{xx}(\hat{\sigma}) - \frac{\hat{\sigma}}{E}\right) \qquad \text{(A-14)}$$

With Equation A-14, Equation A-11 becomes

$$\nu_{\text{apparent}} = \frac{\dfrac{\hat{\sigma}\nu_e}{E} + \dfrac{1}{2}\left(\varepsilon_{xx}(\hat{\sigma}) - \dfrac{\hat{\sigma}}{E}\right)}{\varepsilon_{xx}(\hat{\sigma})} \qquad \text{(A-15)}$$

which may be rearranged to

$$\nu_{\text{apparent}} = \frac{\hat{\sigma}}{\varepsilon_{xx}(\hat{\sigma})}\left(\frac{\nu_e - \dfrac{1}{2}}{E}\right) + \frac{1}{2} \qquad \text{(A-16)}$$

In Equation A-16, ν_e and E are experimentally determined from linear elastic region data for the material under test, $\hat{\sigma}$ and $\varepsilon_{xx}(\hat{\sigma})$ are the longitudinal stress and longitudinal strain at stress $\hat{\sigma}$, and ν_{apparent} is the predicted Poisson's ratio at these values. Equation A-16 is equivalent to Equation 1 of the text.

*See, e.g., Table II of this report.

DISTRIBUTION LIST

No. of Copies	Organization	No. of Copies	Organization
2	Commander Defense Documentation Center ATTN: DDC-TCA Cameron Station Alexandria, VA 22314	2	Commander US Army Missile Command ATTN: DRSMI-R DRSMI-RBL Redstone Arsenal, AL 35809
1	Director Defense Advanced Research Projects Agency ATTN: Tech Info 1400 Wilson Boulevard Arlington, VA 22209	1	Commander US Army Tank Automotive Development Command ATTN: DRDTA-RWL Warren, MI 48090
1	Commander US Army Materiel Development and Readiness Command ATTN: DRCDMA-ST 5001 Eisenhower Avenue Alexandria, VA 22333	2	Commander US Army Mobility Equipment Research & Development Command ATTN: Tech Docu Cen, Bldg 315 DRSME-RZT Fort Belvoir, VA 22060
1	Commander US Army Aviation Systems Command ATTN: DRSAV-E 12th and Spruce Streets St. Louis, MO 63166	1	Commander US Army Armament Command Rock Island, IL 61202
1	Director US Army Air Mobility Research and Development Laboratory Ames Research Center Moffett Field, CA 94035	1	Commander US Army Watervliet Arsenal ATTN: Dr. F. Schneider Watervliet, NY 12189
2	Commander US Army Electronics Command ATTN: DRSEL-RD DRSEL-HL-CT/S. Crossman Fort Monmouth, NJ 07703	1	Commander US Army Harry Diamond Laboratories ATTN: DRXDO-TI 2800 Powder Mill Road Adelphi, MD 20783
1	Commander US Army Electronic Proving Ground ATTN: Tech Lib Fort Huachuca, AZ 85613	5	Commander US Army Materials and Mechanics Research Center ATTN: DRXMR-ATL DRXMR-T/J. Bluhm DRXMR-XH/J. Dignam DRXMR-XO/E. Hagge DRXMR-XP/Dr. J. Burke Watertown, MA 02172

27

DISTRIBUTION LIST

No. of Copies	Organization	No. of Copies	Organization
1	Commander US Army Natick Research and Development Command ATTN: DRXRE/Dr. D. Sieling Natick, MA 01762	1	Director US Army Ballistic Missile Defense Program Office 1320 Wilson Boulevard Arlington, VA 22209
1	Director US Army TRADOC Systems Analysis Activity ATTN: ATAA-SA White Sands Missile Range NM 88002	1	Commander US Army War College ATTN: Lib Carlisle Barracks, PA 17013
1	HQDA (DAMA-ARP-P/Dr. Watson) Washington, DC 20310	1	Commander US Army Command and General Staff College ATTN: Archives Fort Leavenworth, KS 66027
1	HQDA (DAMA-ARP) Washington, DC 20310	1	Mathematics Research Center US Army University of Wisconsin Madison, WI 53706
1	HQDA (DAMA-MS) Washington, DC 20310		
1	Deputy Assistant Secretary of the Army (R&D) Department of the Army Washington, DC 20310	3	Commander US Naval Air Systems Command ATTN: AIR-604 Washington, DC 20360
1	Commander US Army Research Office P.O. Box 12211 Research Triangle Park NC 27709	3	Commander US Naval Ordnance Systems Command ATTN: ORD-0632 ORD-035 ORD-5524 Washington, DC 20360
1	Director US Army BMD Advanced Technology Center ATTN: CRDABH-R/W. Loomis P.O. Box 1500/West Station Huntsville, AL 35807	1	Office of Naval Research ATTN: Code 402 Department of the Navy Washington, DC 20360
1	Commander Ballistic Missile Defense Systems Command ATTN: SENSC/Mr. Davidson P.O. Box 1500 Huntsville, AL 35807	1	Commander US Naval Surface Weapons Center ATTN: Code Gr-0/Dr. W. Soper Dahlgren, VA 22448

DISTRIBUTION LIST

No. of Copies	Organization	No. of Copies	Organization
1	Commander and Director US Navy Electronics Lab ATTN: Lib San Diego, CA 92152	7	Sandia Laboratories ATTN: Dr. L. Davison Div 5163 Dr. C. Harness H. J. Sutherland Code 5133 Code 1721 Dr. P. Chen Albuquerque, NM 87115
3	Director US Naval Research Laboratory ATTN: Code 5270 Mr. F. MacDonald Code 2020/Tech Lib Code 7786/J. Baker Washington, DC 20360		
1	AFATL (DLDL/MAJ J. E. Morgan) Eglin AFB, FL 32542	5	Brown University Division of Engineering ATTN: Prof R. Clifton Prof H. Kolsky Prof A. Pipkin Prof P. Symonds Prof J. Martin Providence, RI 02192
1	RADC (EMTLD/Lib) Griffiss AFB, NY 13440		
1	AUL (3T-AUL-60-118) Maxwell AFB, AL 36112	5	California Institute of Technology Division of Engineering and Applied Science ATTN: Dr. J. Milowitz Dr. E. Sternberg Dr. J. Knowles Dr. T. Coguhey Dr. R. Shield Pasadena, CA 91102
1	Director Jet Propulsion Laboratory ATTN: Lib (TDS) 4800 Oak Grove Drive Pasadena, CA 91103		
1	Director National Aeronautics and Space Administration Manned Spacecraft Center ATTN: Lib Houston, TX 77058	4	Carnegie Mellon University Department of Mathematics ATTN: Dr. D. Owen Dr. M. E. Gurtin Dr. B. Coleman Dr. W. Williams Pittsburg, PA 15213
1	Director Environmental Science Service Administration US Department of Commerce Boulder, CO 80302	1	Catholic University of America School of Engineering and Architecture ATTN: Prof A. Durelli Prof J. McCoy Washington, DC 20017
1	DuPont Experimental Labs ATTN: Mr. J. Lupton Wilmington, DE 19801		

29

DISTRIBUTION LIST

No. of Copies	Organization	No. of Copies	Organization

4	Cornell University
	Department of Theoretical
	  Applied Mechanics
	ATTN: Prof E. Cranch
	      Prof G. Ludford
	      Prof D. Robinson
	      Prof Y-H Pao
	Ithaca, NY 14850
		1	Michigan State University
			College of Engineering
			ATTN: Prof W. Sharpe
			East Lansing, MI 48823

1	Harvard University Division of Engineering and Applied Physics ATTN: Dr. G. Carrier Cambridge, MA 02138	1	New York University Department of Mathematics ATTN: Dr. J. Keller University Heights New York, NY 10053
2	Iowa State University Engineering Research Laboratory ATTN: Dr. G. Nariboli Dr. A. Sedov Ames, IA 50010	1	North Carolina State University School of Engineering ATTN: Dr. T. SunChang Raleigh, NC 27607

5	The Johns Hopkins University
	ATTN: Dr. J. Ericksen
	      Dr. J. Bell
	      Dr. R. Green
	      Dr. C. Truesdell
	      Dr. R. Pond
	34th and Charles Streets
	Baltimore, MD 21218
		1	North Carolina State University
			Department of Engineering
			  Mechanics
			ATTN: Dr. W. Gingham
			P.O. Box 5071
			Raleigh, NC 27607

3	Lehigh University
	Center for the Application
	  of Mathematics
	ATTN: Dr. E. Varley
	      Dr. R. Rivlin
	      Prof M. Mortell
	Bethlehem, PA 18015
		2	Pennsylvania State University
			Engineering Mechanical Dept
			ATTN: Dr. E. N. Haythornthwaite
			      Prof N. Davids
			University Park, PA 16802

1	Massachusetts Institute
	  of Technology
	ATTN: Dr. R. Probstein
	77 Massachusetts Avenue
	Cambridge, MA 02139
		2	Forrestal Research Center
			Aeronautical Engineering Lab
			Princeton University
			ATTN: Dr. S. Lam
			      Dr. A. Eringen
			Princeton, NJ 08540

		1	Purdue University Institute for Mathematical Sciences ATTN: Dr. E. Cumberbatch Lafayette, IN 47907

DISTRIBUTION LIST

No. of Copies	Organization	No. of Copies	Organization
2	Rice University ATTN: Dr. R. Bowen Dr. C. C. Wang P.O. Box 1892 Houston, TX 77001	1	University of California Department of Mechanics ATTN: Dr. R. Stern 504 Hilgard Avenue Los Angeles, CA 90024
1	Southern Methodist University Solid Mechanics Division ATTN: Prof H. Watson Dallas, TX 75221	1	University of Delaware Department of Mechanical Engineering ATTN: Prof J. Vinson Newark, DE 19711
2	Southwest Research Institute Dept of Mechanical Sciences ATTN: Dr. U. Lindholm Dr. W. Baker 8500 Culebra Road San Antonio, TX 78228	3	University of Florida Dept of Engineering Mechanics ATTN: Dr. R. Fosdick Minneapolis, MN 55455
1	Stanford Research Institute Poulter Laboratory 333 Ravenswood Avenue Menlo Park, CA 94025	1	University of Notre Dame Department of Metallurgical Engineering and Materials Sciences ATTN: Dr. N. Fiore Notre Dame, IN 46556
1	Stanford University ATTN: Dr. E. H. Lee Stanford, CA 94305	1	University of Pennsylvania Towne School of Civil and Mechanical Engineering ATTN: Prof Z. Hashin Philadelphia, PA 19105
1	Tulane University Dept of Mechanical Engineering ATTN: Dr. S. Cowin New Orleans, LA 70112	4	University of Texas Dept of Engineering Mechanics ATTN: Prof H. Calvit Dr. M. Stern Dr. M. Bedford Prof Ripperger Austin, TX 78712
2	University of California ATTN: Dr. M. Carroll Dr. P. Naghdi Berkeley, CA 94704		
1	University of California Dept of Aerospace and Mechanical Engineering Sciences ATTN: Dr. Y. C. Fung P.O. Box 109 La Jolla, CA 92037		Aberdeen Proving Ground Marine Corps Ln Ofc Dir, USAMSAA

31